# A Molecular Modeling Investigation of Cation and Water Siting in Crystalline Silicotitanates

**James P. Larentzos,[†] Abraham Clearfield,[‡] Akhilesh Tripathi,[‡] and Edward J. Maginn*[,†]**

*Department of Chemical and Biomolecular Engineering, University of Notre Dame, 182 Fitzpatrick Hall, Notre Dame, Indiana 46556-5637, and Department of Chemistry, Texas A&M University, College Station, Texas 77842-3012*

*Received: July 5, 2004; In Final Form: September 1, 2004*

A classical rigid ion force field potential has been developed for simulations involving $Na^+$, $Cs^+$, and water in cystalline silicotitanate (CST) and 25% niobium-substituted crystalline silicotitantate (Nb−CST) materials. The siting of the cations and water predicted by the force field agree favorably with experimental powder X-ray diffraction results. The accuracy and performance of the rigid ion model are compared against results obtained using a polarizable shell model potential. The rigid ion model yields comparable accuracy at a fraction of the computational cost of the shell model. The simulations provide insight into the organization and hydration of the cations in the CST materials and help explain the large selectivity these materials show for $Cs^+$ ion exchange.

## 1. Introduction

Separation of selected radionuclides from high-level nuclear waste solutions is a vital step to minimize disposal volume. A number of inorganic ion exchangers have been shown to selectively remove ions in the presence of high radiation fields.[1] In particular, crystalline silicotitanates (hereafter referred to as CST) are currently under consideration for the separation of $^{137}Cs$ from nuclear waste solutions stored at various U.S. Department of Energy facilities. A wealth of experimental studies have been conducted to characterize the CST structure to better understand its ion exchange properties.[2−6] In designing a more cost-effective process, the development of improved ion exchangers with increased capacity, selectivity, and kinetics is desired. It is possible to enhance the ion exchange performance by introducing suitable structural modifications. For example, partial substitution of niobium for titanium in the CST framework has been shown to improve selectivity for cesium.[7,8] To develop new materials with improved ion exchange performance, as well as understand the performance trends of existing materials, it is important to gain a fundamental understanding of the dominant interactions between the framework structure and the exchanging cations and water molecules. With such knowledge, one can begin to accurately predict and optimize ion exchange performance while adjusting heteroatom (Nb, Ge, Ta) substitutions, the degree of hydration, and the countercation (Cs, Sr, and various other actinides) compositions.

Molecular simulation methods have the potential to be a valuable tool in guiding future synthesis efforts.[9−11] First principles methods, such as ab initio molecular dynamics[12] and quantum mechanics/molecular mechanics embedded cluster methods,[13] have been used recently to examine water in Ti-containing zeolites. The advantage of these approaches is their accuracy and predictive capability. Unfortunately, the computational requirements involved in these techniques is quite high, especially for the ab initio molecular dynamics. Consequently, these methods are typically applied to small systems and only over very short time scales. To overcome the limitations of first principles simulations, classical modeling approaches may be used. Techniques such as energy minimization,[14] molecular dynamics,[15] and Monte Carlo[16] have been used extensively and with great success to model guest species in porous crystalline materials such as zeolites,[17] porous carbon,[18] mesoporous silica,[19] and dehydrated titanosilicates,[20,21] the latter of which are structurally related to the CST materials. In addition, lattice energy minimizations have been conducted to predict cation sites in dehydrated titanosilicate ETS-10.[22,23] The accuracy of the classical simulations depends on the quality of the intermolecular force field used to describe the energetic interactions present in the system. Therefore, the development of accurate force fields for guest species in porous materials is an important and ongoing research activity.

Several different types of force field potentials have been used to study guest species in porous crystalline materials. A number of studies have utilized a shell model potential,[24] which captures polarization effects between framework atoms and guest species by representing atoms as a massless "shell" tethered to an atomic "core". The shell represents the electronic charge cloud of the atom, and the polarizability of the atom is governed by the strength of the tethering potential and overall charge on the core and shell. The shell model has been used to examine lattice relaxation effects, crystal structure, and preferred cation locations in various dehydrated zeolites.[25,26] A water force field consistent with the shell model has been developed[27] and applied to predict cation and water positions in zeolites as well as examine lattice relaxation effects.[28,29]

While these previous studies demonstrate the effectiveness of the shell model, it has drawbacks. First, the computational cost of the shell model is high. Besides increasing the number of interaction sites present in the system, the massless shells require additional thermal equilibration moves in Monte Carlo (MC) or special treatment when using molecular dynamics

* Corresponding author. Phone: (574) 631-5687. Fax: (574) 631-8366. E-mail: ed@nd.edu

[†] University of Notre Dame.

[‡] Texas A&M University.

10.1021/jp047041s CCC: $27.50 
Published on Web 10/19/2004

(MD). To enable the acceleration of the shell to be finite in an MD simulation, a small mass can be added to the shells, or the shell positions updated by energy minimization between each molecular dynamics time step. Both schemes greatly increase computational cost. Second, the shell model has been shown to suffer from convergence problems when examining hydrated zeolite structures.[30]

Rigid ion models have also been used to model guest species in porous materials. These models, which utilize effective partial charges on the atoms and neglect polarization, do surprisingly well for many systems. For example, models have been developed which accurately predict cation location in dehydrated zeolites, such as faujasite[31−36] and zeolite 5A[37] at a fraction of the computational cost of the shell model. Ethanol/water adsorption in the zeolite NaA[38] and water dynamics in zeolite 4A have also been investigated.[39] A key requirement for these models is that the dispersion-repulsion interactions and partial charges be appropriately parameterized to yield "effective" two-body potentials that account in an approximate way for polarization effects.

The objective of the present work is to develop and utilize a rigid ion model for simulating the siting of $Na^+$, $Cs^+$, and water in CST and Nb-substituted CST materials. The latter material consists of regular CST but with Nb partially substituted for Ti. We are unaware of any previous modeling studies of these systems. The CST class of materials are ideal for developing and testing methods and force fields for ion exchange. This is due to the fact that they have been well characterized by X-ray studies, as described in section 2, although some uncertainty still remains regarding cation location in some materials. Moreover, the location of various cations in the materials depends critically on water association and framework composition. All of these effects can be explored with modeling. Simulated cation and water positions will be compared with experimental X-ray powder diffraction data as well as with limited results obtained from calculations utilizing the shell model potential with parameters optimized for this system. Once validated for CST materials, the force field can be applied to related materials to test for transferability as well as to predict ion exchange performance. This information can be used to help guide efforts of modifying materials as well as synthesizing new materials for use in nuclear waste cleanup.

## 2. Experimental Background

The class of compounds to be treated theoretically in this study are framework structured titanium silicates enclosing a tunnel and its 25% Nb substituted forms. Specifically we consider the compounds of ideal formula $Na_2Ti_2O_3SiO_4 \cdot 2H_2O$ and $Na_{1.5}Nb_{0.5}Ti_{1.5}O_3SiO_4 \cdot 2H_2O$ in which the sodium ions are replaceable by other cations.[2,8] Preparation: 6.66 mL of $TiCl_4$ was slowly added to 23 mL ddi water and 40 mL of 30% $H_2O_2$. To this mixture was added 40 mL of 10 M NaOH followed by 150 mL of ddi $H_2O$ and a solution of 6 mmol $SiO_2$ in 1 M NaOH. A clear solution results to which was then added 0.12 mol of NaOH. The mixture was sealed in a Teflon-lined pressure vessel and kept at 200 °C for 10 days. After cooling, the product was recovered by filtration then washed with 1 M NaOH and ethanol. In the Nb containing phase, 25 mol % of the $TiCl_4$ was replaced by $NbCl_5$.[2,8]

Powder X-ray diffraction analysis reveals that the crystals are tetragonal $a = 7.8082(2)$ Å, $c = 11.9735(4)$ Å, space group $P4_2/mcm$, $Z = 4$. The titanium atoms occur in clusters of four grouped about a $4_2$ axis, two up and two down rotated by 90°. Each titanium is octahedrally coordinated, sharing edges in such a way that an inner core or four oxygens and four Ti atoms form a distorted cubane-like structure.[2] These cubane-type structures are bridged to each other through silicate groups along the *a*- and *b*-axis directions. The titanium−oxygen clusters are 7.81 Å apart in both the *a*- and *b*-axis directions with the Si atoms at $Z = 1/4, 3/4$. In the *c*-axis direction, the Ti atoms are bridged by oxo groups. The *c*-axis is approximately 12 Å long, which is twice the distance from the center of one cubane-like cluster to its neighbor in the *c*-axis direction.

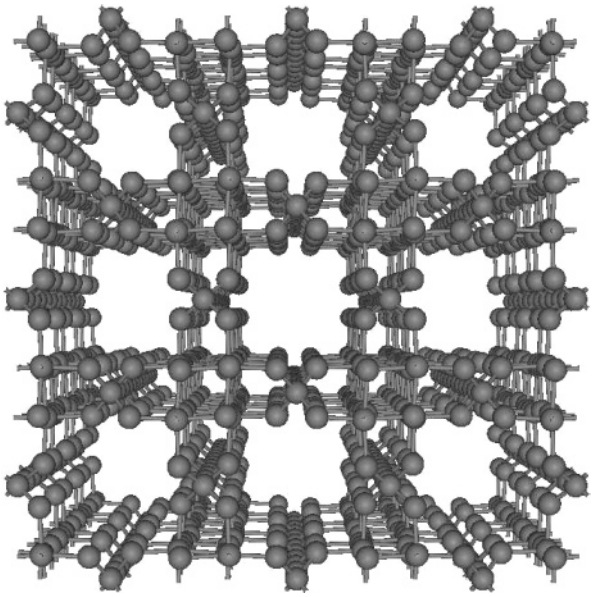

**Figure 1.** 3×3×3 "supercell" of CST viewed along [001]. The CST tunnels are one-dimensional along the *c*-axis.

The net result of this framework arrangement is that tunnels are formed that are one-dimensional, running along the *c*-axis direction (see Figure 1). Perpendicular to the tunnels are vacancies in the faces of four sides of the tunnels. These cavities are just the right size to enclose sodium ions. Four silicate oxygens bond to the sodium ion at a distance of 2.414(5) Å. The sodium ion coordination is completed by bonding to two water molecules in the tunnels at a bond distance of Na−O of 2.765(1) Å. Half of the $Na^+$ ions are thus accounted for in the framework sites as there are two sodiums in each face over one *c*-axis cell length for a total of four out of the eight required per unit cell. The remaining sodiums reside within the tunnels along with water molecules (see Figure 2a).

X-ray diffraction studies indicate that the exchangeable $Na^+$ ions form Na−O bond distances within the tunnel that are longer than the sum of the ionic radii (2.42 Å)[40] at 2.76(1) Å. This bond distance measurement was made with only 64% of the sodium ion sites occupied.[2] The deficiency of sodium arises from hydrolysis during washing so that the actual formula was $Na_{1.64}H_{0.36}Ti_2O_3SiO_4 \cdot 1.8H_2O$. Because of the deficiency of $Na^+$, the sodium ion positions were found to be disordered with partial occupancy by water (or hydronium ions), as listed in Table 1, upper left. It is possible to obtain the fully occupied sodium phase by not washing the product of the hydrothermal reaction with water.

The sodium form was converted to the proton phase by washing with 0.1 M HCl, and this phase was converted to the $Cs^+$ form by addition of a mixture of CsOH and $CsNO_3$. The exchange capacity of the protonic phase is 7.55 meq/L, but the amount of $Cs^+$ taken up was close to 25% of this value. The reason for this low uptake became evident from the crystal structure.[5]

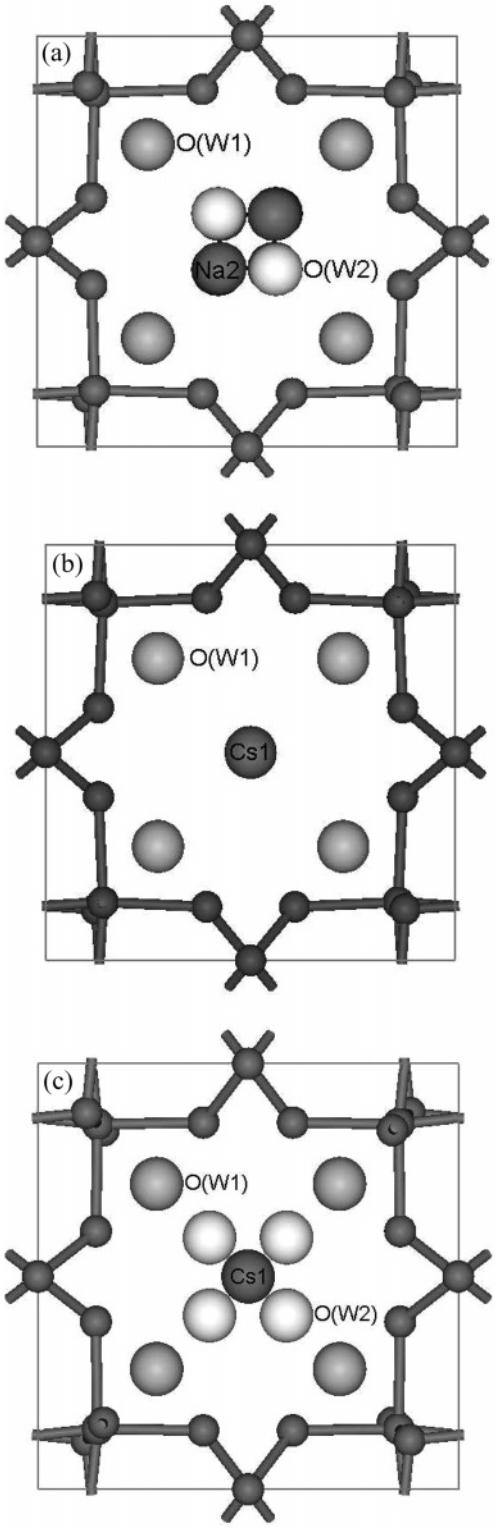


**Figure 2.** Tunnel of (a) Na−CST, (b) Cs−CST, and (c) Cs−Nb−CST viewed along [001]. The experimentally determined exchangeable cation and water sites are shown to reside in the CST tunnels. O(W1) and O(W2) represent the two water sites observed experimentally, while Na2 and Cs1 represent the exchangeable sodium and cesium sites, respectively. The Cs2 sites are not shown because they are located behind the Cs1 sites.

The X-ray data shows that the $Cs^+$ fits snugly within the tunnels at $z$ (or $c$) = 1/4, 3/4, which is shown in Figure 2b and listed in Table 1, upper right. The $Cs^+$ forms eight bonds to the silicate oxygens of 3.183(5) Å[2]. Thus, the Cs−O bonds are very close to the sum of the ionic radii of $Cs^+$ and O.[2,5] Since the $c$-axis dimension is approximately 12 Å, the two cesium ions are 6 Å apart, but the diameter of an 8-coordinate $Cs^+$ is 3.52 Å. Therefore, no additional cesium ions can fit into the tunnel. This fact accounts for the 25% capacity. The large $Cs^+$ also cannot fit into the small framework site at Z = 0, 1/2 when the preferred tunnel sites are occupied. However, $Na^+$ can fit into the framework sites and when a mixed solution of $Na^+$ and $Cs^+$ is exchanged, both types of exchange occur simultaneously. However, the position of $Na^+$ in this case could not be determined experimentally.

In actual waste solutions the CST does not perform well. The solutions are about 6 M in $Na^+$ and 1−3 M in NaOH. Thus, the extremely high level of sodium ion as compared to the low amount of $Cs^+$ in tank wastes ($\sim 10^{-4}$ M) prevents any significant exchange of $Cs^+$. However, if 25 mol % of $Nb^{5+}$ is substituted for $Ti^{4+}$, the selectivity for $Cs^+$ increases and is sufficient for remediation purposes. Solution of the crystal structures of a number of Nb-substituted $Cs^+$ containing CST were performed,[8] and the $Cs^+$ was found to have two sites as listed in Table 1, lower right. The $Cs^+$ and water sites are shown in Figure 2c. The $Cs^+$ in the (1/2, 1/2, 1/4) site is 12-coordinate. This increase in coordination number from 8 to 12 greatly favors an increase in $-\Delta G°$ for the exchange reaction and is responsible for the increase in selectivity observed. In summary, the high level of selectivity by the two forms of CST result from the very strong bonds formed by $Cs^+$ with the framework oxygens and the high coordination numbers. In terms of the ion exchange reaction

$$\overline{RNa^+} + Cs^+(aq) \rightleftharpoons \overline{RCs^+} + Na^+(aq) \qquad (1)$$

where the bars indicate the solid exchanger, the free energy should be highly negative. The $Cs^+$ in the aqueous phase has a low hydration level but in the Nb−CST it is highly hydrated. All twelve bonds to $Cs^+$ are strong bonds, providing a highly exothermic effect. In contrast, $Na^+$ is only weakly bonded in the tunnels and probably less hydrated than in the aqueous phase. Thus, any effect of negative entropy would be small in comparison to the exothermicity of bond formation. Even the 8-coordinate $Cs^+$ shows high selectivity for $Cs^+$ in $Na^+$ solutions of moderate concentration. At high sodium ion concentrations, $Na^+$ also fills tunnel sites, preventing water from bonding to $Cs^+$.

## 3. Simulation Model and Methods

**3.1. Model of CST Structures.** Four different but related CST materials were modeled: sodium exchanged CST (Na−CST); cesium exchanged CST (Cs−CST); 25% niobium-substituted CST (Nb−CST); and cesium exchanged, 25% niobium-substituted CST (Cs−Nb−CST). The experimentally determined composition of each material is given in Table 2, along with the composition used in the modeling. With the exception of the Nb−CST material, modeling the exact experimental composition would require the use of multiple unit cells (a "supercell"), with each unit cell composition varying slightly. Rather than attempt to model the exact experimental composition, a compromise was made in which the composition used was that which most closely matches the overall experimental composition while keeping each unit cell composition the same. This was done for two reasons. First, we only have overall experimental compositions with no knowledge of how the composition of each unit cell can vary within a supercell. Second and most important, we wish to make direct comparison between calculations done with the rigid ion potential and those that

**TABLE 1: Experimental Fractional Atomic Coordinates for Na−CST, Cs−CST, Nb−CST, and Cs−Nb−CST[2,8]**

Na−CST Experimental Atomic Coordinates

| atom | x | y | z | occupancy |
|---|---|---|---|---|
| Ti | 0.1382(2) | 0.1382(2) | 0.1568(2) | 1.00 |
| Si | 0.0000 | 0.5000 | 0.2500 | 1.00 |
| O1 | 0.1301(5) | 0.3934(5) | 0.1692(5) | 1.00 |
| O2 | 0.1210(8) | 0.1210(8) | 0.3325(4) | 1.00 |
| O4 | 0.1377(11) | 0.1377(11) | 0.0000 | 1.00 |
| Na1 | 0.0000 | 0.5000 | 0.5000 | 1.00 |
| Na2 | 0.4351(19) | 0.4351(19) | 0.0598(19) | 0.32 |
| O(W1) | 0.2643(14) | 0.2643(14) | 0.5000 | 1.00 |
| O(W2) | 0.4314(25) | 0.4314(25) | 0.3101(20) | 0.42 |

a = 7.8082(2) Å, *c* = 11.9735(4) Å

Cs−CST Experimental Atomic Coordinates

| atom | x | y | z | occupancy |
|---|---|---|---|---|
| Ti | 0.1401(2) | 0.1401(2) | 0.1570(2) | 1.00 |
| Si | 0.0000 | 0.5000 | 0.2500 | 1.00 |
| O1 | 0.1287(5) | 0.3925(5) | 0.1673(5) | 1.00 |
| O2 | 0.1228(7) | 0.1228(7) | 0.3329(4) | 1.00 |
| O4 | 0.1386(11) | 0.1386(11) | 0.0000 | 1.00 |
| Na1 | 0.0000 | 0.5000 | 0.5000 | 1.00 |
| Cs1 | 0.5000 | 0.5000 | 0.2500 | 0.20 |
| Cs2 | 0.5000 | 0.5000 | 0.131(2) | 0.10 |
| O(W1) | 0.2738(12) | 0.2738(12) | 0.5000 | 1.00 |

a = 7.8258(2) Å, *c* = 11.9815(4) Å

Nb−CST Experimental Atomic Coordinates

| atom | x | y | z | occupancy |
|---|---|---|---|---|
| Ti/Nb | 0.1392(2) | 0.1392(2) | 0.1541(2) | 0.75/0.25 |
| Si | 0.0000 | 0.5000 | 0.2500 | 1.00 |
| O1 | 0.1195(9) | 0.3876(8) | 0.1710(5) | 1.00 |
| O2 | 0.1126(8) | 0.1126(8) | 0.3295(8) | 1.00 |
| O4 | 0.1445(12) | 0.1445(12) | 0.0000 | 1.00 |
| Na1 | 0.0000 | 0.5000 | 0.5000 | 1.00 |
| O(W1) | 0.2744(13) | 0.2744(13) | 0.5000 | 1.00 |
| O(W2) | 0.4479(15) | 0.4479(15) | 0.1117(13) | 0.50 |

a = 7.8331(4) Å, *c* = 12.0074(7) Å

Cs−Nb−CST Experimental Atomic Coordinates

| atom | x | y | z | occupancy |
|---|---|---|---|---|
| Ti/Nb | 0.1418(2) | 0.1418(2) | 0.1528(2) | 0.75/0.25 |
| Si | 0.0000 | 0.5000 | 0.2500 | 1.00 |
| O1 | 0.1382(8) | 0.3935(7) | 0.1675(5) | 1.00 |
| O2 | 0.1154(6) | 0.1154(6) | 0.3344(7) | 1.00 |
| O4 | 0.1486(9) | 0.1486(9) | 0.0000 | 1.00 |
| Na1 | 0.0000 | 0.5000 | 0.5000 | 1.00 |
| Cs1 | 0.5000 | 0.5000 | 0.2500 | 0.30 |
| Cs2 | 0.5000 | 0.5000 | 0.1263(15) | 0.10 |
| O(W1) | 0.2824(12) | 0.2824(12) | 0.5000 | 0.50 |
| O(W2) | 0.5916(25) | 0.5916(25) | 0.5000 | 0.50 |

a = 7.8397(4) Å, *c* = 12.0321(6) Å

**TABLE 2: Experimental and Simulated Composition of the CST Materials**

| | experimental | simulated |
|---|---|---|
| Na−CST | $Na_{1.64}H_{0.36}Ti_2O_3SiO_4 \cdot 1.84H_2O$ | $Na_{1.75}H_{0.25}Ti_2O_3SiO_4 \cdot 1.75H_2O$ |
| Cs−CST | $Na_{1.49}Cs_{0.2}H_{0.31}Ti_2O_3SiO_4 \cdot H_2O$ | $Na_{1.50}Cs_{0.25}H_{0.25}Ti_2O_3SiO_4 \cdot H_2O$ |
| Nb−CST | $H_{0.5}NaNb_{0.5}Ti_{1.5}O_3SiO_4 \cdot 2H_2O$ | $H_{0.5}NaNb_{0.5}Ti_{1.5}O_3SiO_4 \cdot 2H_2O$ |
| Cs−Nb−CST | $Cs_{0.2}H_{0.3}NaNb_{0.5}Ti_{1.5}O_3SiO_4 \cdot H_2O$ | $Cs_{0.25}H_{0.25}NaNb_{0.5}Ti_{1.5}O_3SiO_4 \cdot H_2O$ |

utilize the shell model. While supercell calculations can be done with the rigid ion model, the computational burden of the shell model makes supercell simulations with this model prohibitively expensive.

In all cases, framework atoms (Si, Ti, Nb, O, and the nonexchangeable sodium, designated as Na1) were held rigid at their experimentally determined crystallographic coordinates. While in principle the shell model can be used to model lattice relaxation effects, we were unable to locate a suitable set of parameters that enabled accurate determination of the lattice parameters for these materials. Thus a rigid lattice was modeled, with the only mobile species being the exchangeable cations (Na2, Cs) and water.

In the Nb−CST and Cs−Nb−CST structures, niobium is partially substituted for framework titanium. The niobium atoms are thought to be randomly distributed over the entire system. Therefore, since the niobium and titanium arrangement is uncertain, a "composite" atom is placed in all octahedrally coordinated sites that could be populated by either titanium or niobium. The potential parameters for this composite atom are derived from a composition-weighted average of the potential parameters for titanium and niobium (Buckingham parameters and partial charges (see section 3.2)). This approach of using a composite or average "T-atom" has been used previously with great success in modeling aluminum substitution for silicon in zeolites.[32]

**3.2. Force Field Details.** The rigid ion potential developed here is based in large part on a previous shell model parameterization. Since the objective of the current study was to develop an efficient rigid ion model that was as accurate as the shell model, some simulations were carried out using the shell model to obtain results against which the rigid ion model results could be compared. Thus, a brief description of the shell model is given, along with a summary of the procedures used to determine model parameters. Following this, methods used to determine rigid ion model parameters are described.

*3.2.1. Shell Model Force Field.* The shell model accounts for polarizability effects on all framework and water oxygen atoms in the following manner. Each oxygen atom is modeled as a core and massless shell, where the shell represents the electronic charge cloud of the atom. The core and shell are connected by a harmonic spring, with the spring constant as well as the core and shell charges determined by the atomic polarizability. A full description of the shell model is given elsewhere.[30]

The total potential energy of the system, $V_{total}$ is obtained by summing all pairwise interactions according to the following expression:

$$V_{total} = V_{CF} + V_{CC} + V_{CW} + V_{WF} + V_{WW} + V_{W} \quad (2)$$

where $V_{CF}$ is the energy due to the cation−framework interaction, $V_{CC}$ is the cation−cation interaction energy, $V_{CW}$ is the cation−water interaction energy, $V_{WF}$ is the water−framework interaction energy, $V_{WW}$ is the water−water interaction energy, and finally, $V_W$ is the intramolecular energy of the water molecules. The cation−framework, cation−water, and water−framework interactions are modeled by combining a Buckingham nonbonded potential and a Coulombic potential. The functional form is given by

$$V_{ij} = A_{ij} \exp\left(\frac{-r_{ij}}{\rho_{ij}}\right) - \frac{C_{ij}}{r_{ij}^6} + \frac{q_i q_j}{r_{ij}} \quad (3)$$

where $V_{ij}$ is the potential energy resulting from the pairwise interaction between atoms $i$ and $j$, $r_{ij}$ is the separation distance between atoms $i$ and $j$, $A_{ij}$, $\rho_{ij}$, and $C_{ij}$ are the Buckingham parameters, and $q_i$ is the charge on atom $i$. Following the Kiselev convention,[41] the framework Si, Ti, and Nb dispersion−replusion interactions with the cations and hydrogen atoms of the water molecules are assumed to be screened by the framework oxygen atoms, and are therefore neglected. The cation−cation interactions are treated as purely Coulombic.

Buckingham parameters for sodium interaction with the framework oxygen atoms were taken from the zeolite simulations of Higgins and co-workers[26] and used without modification. The cesium parameters from this work were too repulsive for accurately modeling the Cs−CST system. Therefore, a new set of parameters were developed by fitting the Buckingham parameters to the experimentally determined binding distance between cesium and framework O1 oxygen atoms in Cs−CST.

The water model developed by de Leeuw and Parker was used.[27] Because it is a nonstandard model, a brief description is given here. The water−water intermolecular interaction is composed of two parts. The intermolecular potential energy between the oxygen atoms of two water molecules is given by a standard 12−6 Lennard-Jones plus Coulombic potential

$$V_{ij} = \frac{A_{ij}}{r_{ij}^{12}} - \frac{B_{ij}}{r_{ij}^{6}} + \frac{q_i q_j}{r_{ij}} \qquad (4)$$

where each oxygen center carries a partial charge $q$. The intermolecular interaction between the oxygen atom of one water molecule and the hydrogen atom of a different water molecule is given by a Buckingham plus Coulombic potential (eq 3). Intramolecular water interactions are treated using a Morse potential for bond stretches and a harmonic potential for bond angle bending. Finally, a 50% intramolecular Coulombic subtraction between the $O_W-H_W$ and $H_W-H_W$ is included.

The cation−water and water−framework dispersion-repulsion interactions were originally derived by Higgins et al.[28] Subsequently, Lewis et al.[29] modified the water−framework interactions by increasing the repulsive term of the Buckingham potential in order to prevent short, unfeasible distances that may arise between water and framework atoms. Therefore, this same strategy was applied to the Ti−O Buckingham parameters of Jentys and Catlow[21] to obtain the interaction parameters between Ti and water.

Finally, each framework atom carries its formal charge. Protons are modeled by assuming they are completely delocalized, and thus their charge is smeared over all framework oxygen shells. A complete listing of the potential parameters and charges is given in Table 3.

*3.2.2. Rigid Ion Potential.* Development of a simple and reliable rigid ion model with accuracy comparable to the shell model is desirable because of the tremendous reduction in computational cost that comes with rigid ion simulations. Jaramillo and Auerbach (JA) have proposed a sodium cation Buckingham potential that has been used with a rigid ion model to determine preferred cation positions in dehydrated faujausite zeolites.[31−33] We adopt the JA sodium Buckingham parameters and proceed by developing consistent Buckingham potential parameters for cesium. The cesium $\rho_{ij}$ Buckingham parameter is constrained to the value derived by Higgins et al., while the cesium $A_{ij}$ and $C_{ij}$ Buckingham parameters were systematically varied until an accurate prediction of cesium positions in Cs−CST was obtained. In addition, the Nb−O Buckingham parameters were taken from Woodley et al.[42] and used to obtain the average T-atom potential for the interaction with water. For water−water interactions, the same Lennard-Jones parameters that were used in the shell model were used in the rigid ion model. Similarly, the shell model bond stretching Morse parameters and bond angle bending harmonic parameters were also used. The shell model Buckingham parameters governing cation−water and water−framework repulsion-dispersion interactions were slightly modified to make them less attractive.

**TABLE 3: Shell Model Parameters**[a]

| Buckingham potential parameters | | | |
|---|---|---|---|
| | $A$ (eV) | $\rho$ (Å) | $C$ (eV Å$^6$) |
| Na−O | 5836.814 | 0.2387 | 0.000 |
| Na−$O_W$ | 4088.384 | 0.2387 | 0.000 |
| Cs−O | 264.354 | 0.3911 | 0.000 |
| Cs−$O_W$ | 264.354 | 0.3911 | 0.000 |
| O−$O_W$ | 22764.000 | 0.1490 | 28.920 |
| Si−$O_W$ | 1283.907 | 0.32052 | 10.66158 |
| Ti−$O_W$ | 760.470 | 0.3879 | 0.000 |
| $T_{AVG}$-$O_W$ | 1326.149 | 0.365925 | 0.000 |
| $H_W$-O | 396.270 | 0.2300 | 0.000 |
| $H_W$-$O_W$ | 396.270 | 0.2500 | 10.000 |

| Lennard-Jones potential parameters | | |
|---|---|---|
| | $A$ (eV Å$^{12}$) | $B$ (eV Å$^6$) |
| $O_W-O_W$ | 39344.98 | 42.15 |

| Morse potential parameters | | | |
|---|---|---|---|
| | $D$ (eV) | $a$ (Å$^{-1}$) | $r_0$ (Å) |
| $H_W-O_W$ | 6.203713 | 2.22003 | 0.92376 |

| Three-body potential parameters | | |
|---|---|---|
| | $k$ (eV rad$^{-2}$) | $\theta_0$ |
| $H_W-O_W-H_W$ | 4.19980 | 108.693195 |

| Coulombic and core−shell spring parameters | | |
|---|---|---|
| | charge (e) | spring (eV Å$^{-6}$) |
| $O_{core}$ | 0.86902 | 74.92 |
| $O_{shell}$ | −2.86902 | |
| $O_{Wcore}$ | 1.250 | 209.449602 |
| $O_{Wshell}$ | −2.050 | |
| $H_W$ | 0.400 | |
| Si | 4.000 | |
| Ti | 4.000 | |
| $T_{AVG}$ | 4.250 | |
| Na | 1.000 | |
| Cs | 1.000 | |

| Intramolecular Coulombic subtraction(%) | |
|---|---|
| $H_W-H_W$ | 50 |
| $H_W-O_W$ | 50 |

[a] The charges do not include the adjustments due to protons.

Partial charges were determined for water by combining the core and shell charges on the oxygen to give a rigid ion water with partial charges of +0.4 e on each hydrogen and −0.8 e on oxygen. The remaining partial charges for each atom type (Si, Ti, Nb, $O_{Si}$, $O_{Ti}$, Na, Cs) were allowed to vary, subject to the following constraints and conditions: (1) sodium and cesium cations are required to carry a formal +1 charge; (2) the charge of Nb must satisfy the relation $q_{Nb} = q_{Ti} + 1$; therefore, in a 25% niobium-substituted material, the average "T-atom" charge is $q_{Tavg} = q_{Ti} + 0.25$; (3) the charge of $O_{Si}$ must satisfy the relation $q_{Si} + 2q_{OSi} = 0$, thereby maintaining local charge neutrality for $SiO_2$ units; (4) because there are various types of oxygen bridges in the CST framework, different charges were permitted for oxygen atoms bridging two titanium atoms by oxo groups or three titanium atoms in the $Ti_4O_4$ clusters ($O_{Ti}$), and oxygen atoms bridging one titanium and one silicon through

**TABLE 4: Force Field Parameters for Rigid Ion Model[a]**

| Buckingham potential parameters | | | |
|---|---|---|---|
| | $A$ (eV) | $\rho$ (Å) | $C$ (eV Å$^6$) |
| Na−O | 5270.814 | 0.2468 | 66.000 |
| Na−$O_W$ | 5270.814 | 0.2468 | 66.000 |
| Cs−O | 8000.000 | 0.3911 | 3000.000 |
| Cs−$O_W$ | 8000.000 | 0.3911 | 3000.000 |
| Nb−$O_W$ | 3023.184 | 0.3000 | 0.000 |
| O−$O_W$ | 22764.000 | 0.1490 | 13.000 |

| Coulombic parameters | |
|---|---|
| | charge (e) |
| $O_{Si}$ | −1.200 |
| $O_{Ti}$ | −1.467 |
| $O_W$ | −0.800 |
| $H_W$ | 0.400 |
| Si | 2.400 |
| Ti | 2.400 |
| Nb | 3.400 |
| $T_{AVG}$ | 2.650 |
| Na | 1.000 |
| Cs | 1.000 |

[a] The charges do not include the adjustments due to protons.

silicate groups ($O_{Si}$); (5) the charge of $O_{Ti}$ is determined by satisfying charge neutrality requirements.

Given these constraints, the charges of framework Si and Ti were systematically varied from +2.0 to +2.4 in 0.05 increments. These different charge sets were then tested on the Nb−CST systems by performing simulated annealing molecular dynamics (see section 3.3) and computing water locations. The Nb−CST system was chosen as a benchmark mainly because there are no moveable cations present (only water molecules) and all framework atoms, including Nb, can be tested at once. As might be expected, more than one charge set was able to predict water positions to within 0.5 Å of the experimental value in Nb−CST. These charge sets were then further tested on the three remaining CST structures. The charge set that best predicted the experimental details of all structures, subject to the five constraints, was then selected. A complete listing of all parameters for the rigid ion model is given in Table 4.

**3.3. Simulation Details.** Due to the sluggish nature of cation motion in these systems under ambient conditions, conventional MD simulations are not well suited for computing cation and water siting. Alternative simulation strategies, such as replica exchange Monte Carlo,[35,43] are required to overcome sampling limitations. Similar results can be obtained using a "simulated annealing" protocol, in which MC or MD simulations are initially conducted at high temperatures where cation mobility is facile. Independent trajectories are then quenched to 300 K to locate preferred cation and water positions.[32,33] We have adopted the simulated annealing approach here, in which the MD simulations are started at 1050 K or higher and slowly cooled to 300 K, at which point the cation and water sites are analyzed. For the shell model, a single quench of one unit cell was performed. For the rigid ion model, one quench was performed on an 18-unit cell system, and results were averaged over all 18 unit cells.

All simulations were performed using the General Utility Lattice Program (GULP).[44] Simulations were conducted in the canonical ensemble using a leapfrog finite difference algorithm with full periodic boundary conditions and a 1 fs time step. Total simulation times were at least 500 ps, with configurations output every 0.25 ps for analysis. A cutoff of 11.2 Å was used and Coulombic forces are evaluated with the Ewald summation.[45] In performing MD simulations with the shell model, the positions of the massless shells were updated after each time step by performing an energy minimization on the shells. This procedure greatly increases the computational burden of the simulations, thus limiting the system size that can be examined with the shell model to a single unit cell. Shell model simulations of one CST unit cell for 500 ps required nearly 5 days of processor time on a 1.4 GHz Pentium III machine. The same length simulation on an 18-unit cell "supercell" took 10 days using the rigid ion model, thus pointing out the large difference in speed between the two models.

## 4. Results and Discussion

The main results of the simulations are the location of cations and water in fractional coordinates, which can be compared directly with experimental results. The following procedure was used for computing the fractional coordinates. For each quenched configuration from the MD trajectory, cation and water coordinates were translated into the central unit cell and classified by the nearest experimental site (within a 2.0 Å cutoff). Next, all cations/water of a particular experimental site were transformed by application of the $P4_2/mcm$ symmetry operation to the position closest to the asymmetric unit cell site that is represented by the experimental crystallographic coordinates in Table 1. The positions of all cation/water species were averaged to yield the simulated fractional coordinates presented in Table 5 and Table 6. The deviation from experiment and standard deviation are also included, where the standard deviation is computed by monitoring the fluctuations about the mean position. Its magnitude gives an indication of the relative mobility of the species. Finally, the simulated fractional coordinates were "idealized" to the special positions that arise due to symmetry constraints and are denoted by asterisks in Table 5 and Table 6. In all cases, the translation distance to the special positions were significantly less than the standard deviations reported.

Distribution plots of cation and water positions are shown in Figure 3, Figure 4, and Figure 7. The distribution plots show the location and motion of the cations and water molecules within the CST tunnels. They are created by discretizing the unit cell into 100 × 100 binning boxes. The cations and water molecules of each configuration from the MD trajectory are categorized into a binning box based on their 2-D position (i.e., $x-y$, $x-z$, or $y-z$ coordinates). Each box is then color coded according to the relative probability that it is occupied by a particular atom type. The relative probability is determined by dividing the number of atoms in each box by the number of atoms in the most populated box. Therefore, the highest populated box is assigned a value of 10 and color coded with the most intense color. The remaining boxes are color coded accordingly.

**4.1. Na-CST.** As discussed in section 2, there are two experimental sodium sites in the Na−CST material, designated Na1 and Na2, and two water sites, O(W1) and O(W2). The nonexchangeable Na1 sodium sites are located in the CST framework, while the exchangeable Na2 sodium sites are located in the CST tunnels. The experimental positions of the exchangeable cations and water molecules can be seen in Figure 2a. Recall that since the Na1 sodium cations are considered to be framework atoms, they are constrained to their experimentally determined atomic coordinates during the simulations.

The fractional coordinates of cations and water molecules for Na−CST predicted from the simulations using the rigid ion model are given in Table 5. Also shown are simulation results in which the shell model potential was used. The rigid ion and

**TABLE 5: Simulated Shell Model and Rigid Ion Model Fractional Atomic Coordinates in Na−CST and Cs−CST[a]**

| Na−CST Shell Model | | | | | | Na−CST Rigid Ion Model | | | | | |
|---|---|---|---|---|---|---|---|---|---|---|---|
| atom type | *X* | *Y* | *Z* | dev. (Å) | std. dev. (Å) | atom type | *X* | *Y* | *Z* | dev. (Å) | std. dev. (Å) |
| sodium (Na2) | 0.403 | 0.403 | 0.016 | 0.64 | 0.31 | sodium (Na2) | 0.374 | 0.373 | 0.011 | 0.90 | 0.23 |
| sodium (Na2)* | 0.403 | 0.403 | 0.016 | 0.64 | | sodium (Na2)* | 0.374 | 0.374 | 0.011 | 0.89 | |
| water (Na2) | 0.415 | 0.424 | 0.069 | 0.21 | 0.78 | water (Na2) | 0.420 | 0.420 | 0.043 | 0.27 | 0.62 |
| water (Na2)* | 0.420 | 0.420 | 0.069 | 0.20 | | water (Na2)* | 0.420 | 0.420 | 0.043 | 0.27 | |
| water (OW1) | 0.265 | 0.265 | 0.500 | 0.01 | 0.22 | water (OW1) | 0.270 | 0.271 | 0.500 | 0.07 | 0.31 |
| water (OW1)* | 0.265 | 0.265 | 0.500 | 0.01 | | water (OW1)* | 0.271 | 0.271 | 0.500 | 0.07 | |
| water (OW2) | 0.486 | 0.490 | 0.335 | 0.70 | 0.68 | water (OW2) | 0.484 | 0.485 | 0.334 | 0.65 | 0.37 |
| water (OW2)* | 0.488 | 0.488 | 0.335 | 0.69 | | water (OW2)* | 0.485 | 0.485 | 0.334 | 0.65 | |
| sodium (OW2) | 0.422 | 0.433 | 0.322 | 0.16 | 0.33 | sodium (OW2) | 0.388 | 0.388 | 0.332 | 0.55 | 0.30 |
| sodium (OW2)* | 0.428 | 0.428 | 0.322 | 0.15 | | sodium (OW2)* | 0.388 | 0.388 | 0.332 | 0.55 | |
| **Cs−CST Shell Model** | | | | | | **Cs−CST Rigid Ion Model** | | | | | |
| atom type | *X* | *Y* | *Z* | dev. (Å) | std. dev. (Å) | atom type | *X* | *Y* | *Z* | dev. (Å) | std. dev. (Å) |
| cesium (Cs1) | 0.500 | 0.501 | 0.251 | 0.02 | 0.50 | cesium (Cs1) | 0.499 | 0.501 | 0.248 | 0.03 | 0.30 |
| cesium (Cs1)* | 0.500 | 0.500 | 0.250 | 0.00 | | cesium (Cs1)* | 0.500 | 0.500 | 0.250 | 0.00 | |
| sodium (Na2) | 0.438 | 0.437 | 0.059 | | 0.57 | sodium (Na2) | 0.379 | 0.381 | 0.035 | | 0.58 |
| sodium (Na2)* | 0.438 | 0.438 | 0.059 | | | sodium (Na2)* | 0.380 | 0.380 | 0.035 | | |
| sodium (Na3) | 0.457 | 0.457 | 0.317 | | 0.54 | sodium (Na3) | 0.385 | 0.381 | 0.324 | | 0.41 |
| sodium (Na3)* | 0.457 | 0.457 | 0.317 | | | sodium (Na3)* | 0.383 | 0.383 | 0.324 | | |
| water (OW1) | 0.276 | 0.277 | 0.503 | 0.05 | 0.30 | water (OW1) | 0.285 | 0.284 | 0.498 | 0.12 | 0.34 |
| water (OW1)* | 0.277 | 0.277 | 0.500 | 0.04 | | water (OW1)* | 0.285 | 0.285 | 0.500 | 0.12 | |

[a] The deviation between the simulated coordinates and the experimental site coordinates is shown. The experimental site with which comparisons are made is given in parentheses. The asterisks (*) denote the computed "special positions" after applying symmetry constraints.

**TABLE 6: Simulated Rigid Ion Model Cation and Water Fractional Coordinates in Nb−CST and Cs−Nb−CST[a]**

| Nb−CST Rigid Ion Model | | | | | |
|---|---|---|---|---|---|
| atom | *X* | *Y* | *Z* | dev. (Å) | std. dev. (Å) |
| water (OW1) | 0.291 | 0.291 | 0.500 | 0.19 | 0.51 |
| water (OW1)* | 0.291 | 0.291 | 0.500 | 0.19 | |
| water (OW2) | 0.482 | 0.483 | 0.132 | 0.46 | 0.38 |
| water (OW2)* | 0.483 | 0.483 | 0.132 | 0.46 | |
| **Cs−Nb−CST Rigid Ion Model** | | | | | |
| atom | *X* | *Y* | *Z* | dev. (Å) | std. dev. (Å) |
| cesium (Cs1) | 0.500 | 0.500 | 0.251 | 0.01 | 0.20 |
| cesium (Cs1)* | 0.500 | 0.500 | 0.250 | 0.00 | |
| water (OW1) | 0.316 | 0.317 | 0.497 | 0.38 | 0.42 |
| water (OW1)* | 0.317 | 0.317 | 0.500 | 0.38 | |
| water (OW2) | 0.625 | 0.623 | 0.509 | 0.38 | 0.58 |
| water (OW2)* | 0.624 | 0.624 | 0.500 | 0.36 | |

[a] The deviation between the simulated coordinates and the experimental site coordinates is shown. The experimental site with which comparisons are made is given in parentheses. The asterisks (*) denote the computed "special positions" after applying symmetry constraints.

shell model simulations yield very similar results. Both models predict water localized very close to the experimental O(W1) and O(W2) sites. The two models also predict that $Na^+$ resides close to the experimental Na2 position, although the deviation between the predicted and experimental site is smaller for the shell model than the rigid ion model. Interestingly, both models indicate that $Na^+$ can also locate in the O(W2) position as well as the Na2 site. This can be seen in Figure 3, which shows the results of the rigid ion simulations for the relative probability of finding $Na^+$ at a given location. Moreover, both potential models indicate that, in addition to residing at the O(W1) and O(W2) sites, water populates the Na2 site, as seen in Figure 4.

We believe that the simulations may provide a more accurate picture of the actual distribution of water and cations in the system, despite the apparent inconsistency with X-ray data. This is based on the fact that $Na^+$ and water are hard to differentiate in X-ray work, especially based upon powder data, due to their similar electron density and hence similar scattering lengths, and so it is possible that if some $Na^+$ and water would exchange between the two sites, it would not be detected experimentally. Furthermore, the simulation results appear quite reasonable when one examines coordination numbers. For water, the simulations predict full occupancy of the O(W1) site with water, in perfect agreement with experiment. This water coordinates with the framework Na1 cations, and also hydrogen bonds with the O2 framework oxygen atoms. The remaining water populates both the O(W2) site and the Na2 site, where it assists in stabilizing the exchangeable sodium cations. The simulations predict that $Na^+$ populates both the Na2 site and the O(W2) site, where it experiences a very favorable environment, coordinating at 3.14 Å with three water molecules, four framework O1 oxygen atoms and one framework O4 oxygen atom. This can be compared with the coordination environment of $Na^+$ in the Na2 position in Figure 5. Both Na2 and O(W2) sodium sites lead to a higher coordination environment than observed experimentally and suggest that both sites are energetically favorable. Therefore, while the original experiments[5] indicate that the exchangeable sodium and water can be resolved into two sites, simulations show evidence that the experimental Na2 and O(W2) sites may be occupied by both sodium and water.

**4.2. Cs−CST.** In the Cs−CST structure, experiments indicate that there are two cesium sites, Cs1 and Cs2, one nonexchangeable sodium site, Na1, and one water site, O(W1). The cesium sites are mutually exclusive, and thus are partially occupied. The cesium and water sites can be seen in Figure 2b. In addition, there are exchangeable sodium cations present in the tunnels, but it is not possible to characterize them through powder X-ray diffraction due to disorder of the tunnel constituents.[2] Statistical occupancy of sodium atoms and water molecules with similar scattering lengths in nearby sites inhibits their precise and complete determination.

The simulated cation and water fractional coordinates for the shell and rigid ion models are given in Table 5. Once again, the two potential models give very similar results. The simulated cesium cations are located very close to the experimental Cs1 site. The simulated position deviates from experiment by 0.02 Å with the shell model and 0.03 Å with the rigid ion model.

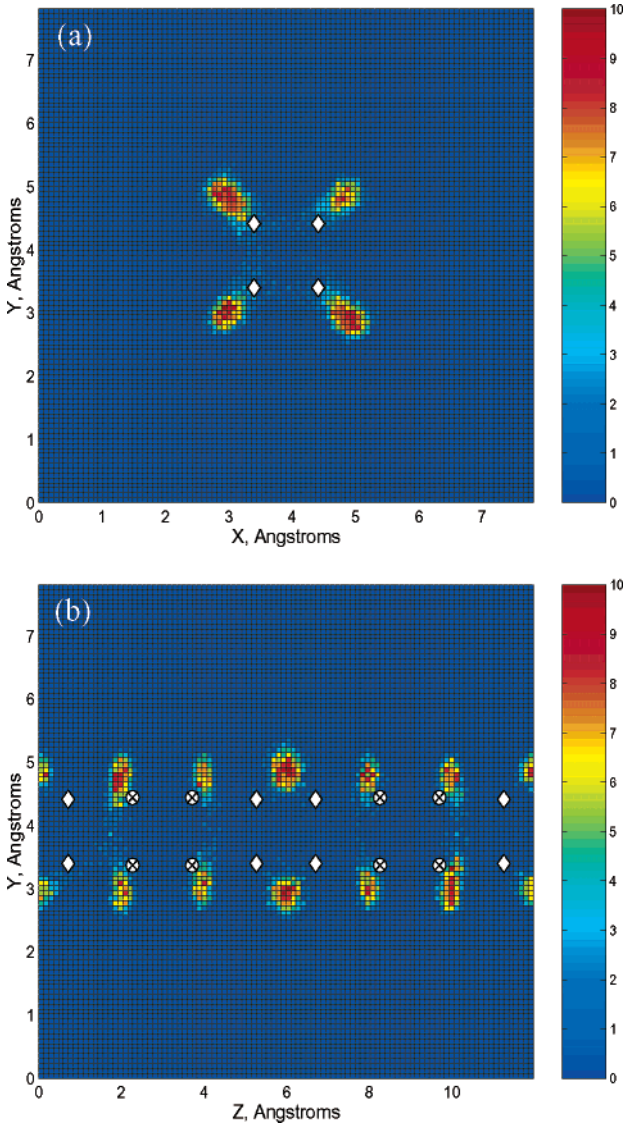


**Figure 3.** Distribution plots of exchangeable sodium cations in one unit cell of Na−CST. Sodium cation plots at 300 K are shown along (a) the [001] direction and (b) the [100] direction. The experimental Na2 and O(W2) sites are represented with diamonds and crossed circles, respectively. Sodium cations are found to occupy both the Na2 and O(W2) experimental sites.

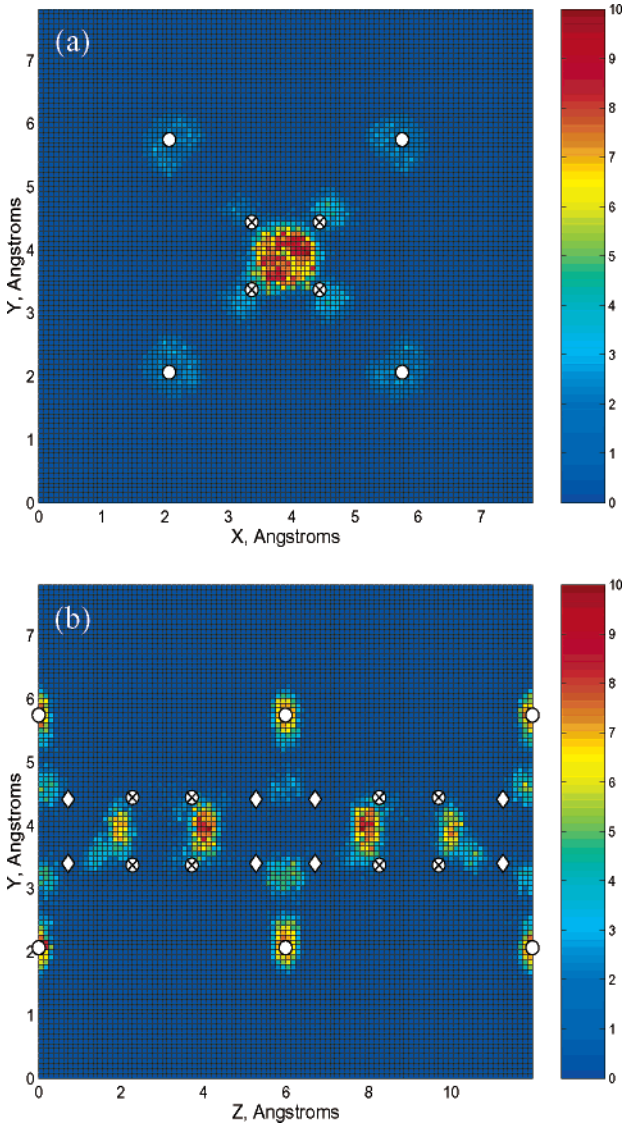


**Figure 4.** Distribution plots of water in one unit cell of Na−CST are shown along (a) the [001] direction and (b) the [100] direction at 300 K. The experimental Na2, O(W1), and O(W2) sites are represented with diamonds, open circles, and crossed circles on the plots, respectively. Water molecules are found to occupy the O(W1) site, as well as the Na2 and O(W2) sites.

Experimentally, the Cs1 position is a highly favorable site because it becomes 8-coordinated with framework O1 oxygen atoms at a distance of 3.18 Å. Figure 6a shows the coordination number of the cesium cations as a function of distance. The simulated cesium cations near site Cs1 coordinate with only 4.3 framework O1 oxygen atoms at a distance of 3.18 Å due to the fact that instantaneous $Cs^+$ positions are slightly shifted away from the experimental position. However, $Cs^+$ does attain an 8-coordination with framework oxygen at a distance of 3.38 Å.

The simulations show no indication of $Cs^+$ locating in the Cs2 sites, although this site is observed experimentally. We believe this discrepancy could be due to a number of factors. First, a uniform composition of cations and water molecules were simulated over all the CST tunnels in the supercell. In real materials, the cation and water compositions within the tunnels may fluctuate about an averaged composition determined through X-ray diffraction. This leads to the possibility of having a "crowded" tunnel where a slight increase in the amount of water and larger cations ($Cs^+$, $Na^+$) may inhibit $Cs^+$ from locating in the Cs1 site, thereby causing $Cs^+$ to locate in the 6-coordinated Cs2 site. A second reason for not observing $Cs^+$ in the Cs2 site could be due to the use of a fixed lattice. Slight distortions to the lattice near $Cs^+$ may take place which are not detected by X-ray diffraction and would not be accounted for in the simulations. Interestingly, both the shell and rigid ion model simulations failed to detect $Cs^+$ in the Cs2 position. This suggests the problem is not with the rigid ion model per se. However, the parameterizations of these models could be the source of discrepancy.

Simulations show the water to be located near the experimental O(W1) site. The deviation from experiment is 0.05 and 0.12 Å for the shell model and rigid ion model, respectively, well within the standard deviations of both simulated positions. The O(W1) water coordinates with nonexchangeable Na1 sodium cations and orients itself such that it hydrogen bonds to the framework O2 oxygen atoms, as in the Na−CST structure.

The exchangeable sodium cations could not be resolved through X-ray diffraction because of the similar X-ray scattering power of $Na^+$ and $H_2O$. The simulations predict that the exchangeable $Na^+$ locates in two sites, designated Na2 and Na3

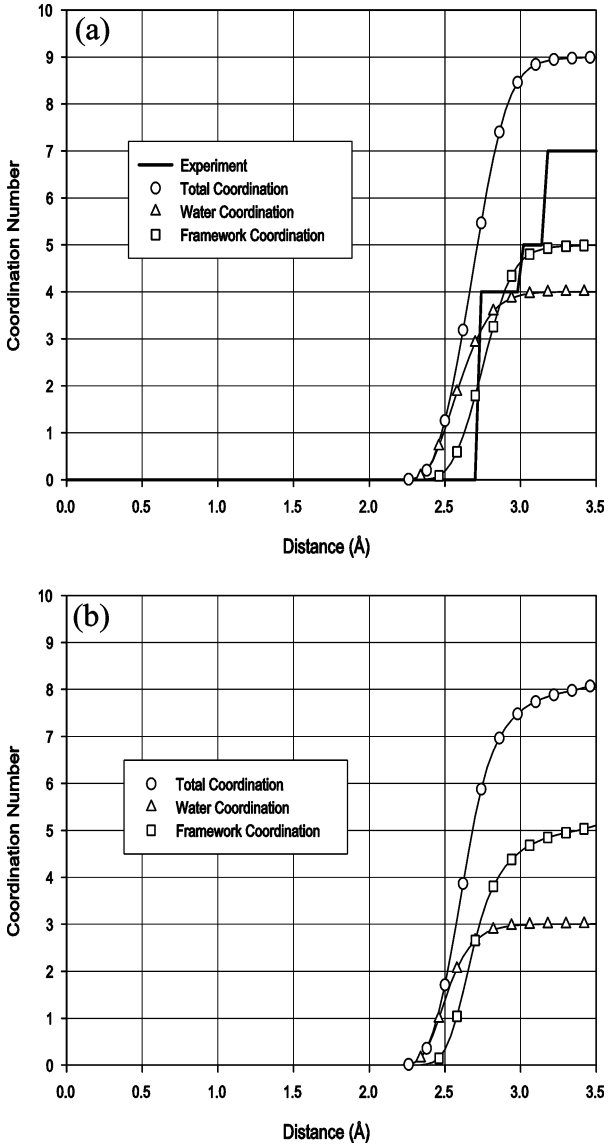


**Figure 5.** Na−CST cation coordination number is plotted as a function of distance. The coordination number of sodium located near the experimental (a) Na2 position and (b) O(W2) positions are shown. The coordination of sodium in the Na2 and O(W2) site is higher than observed experimentally.

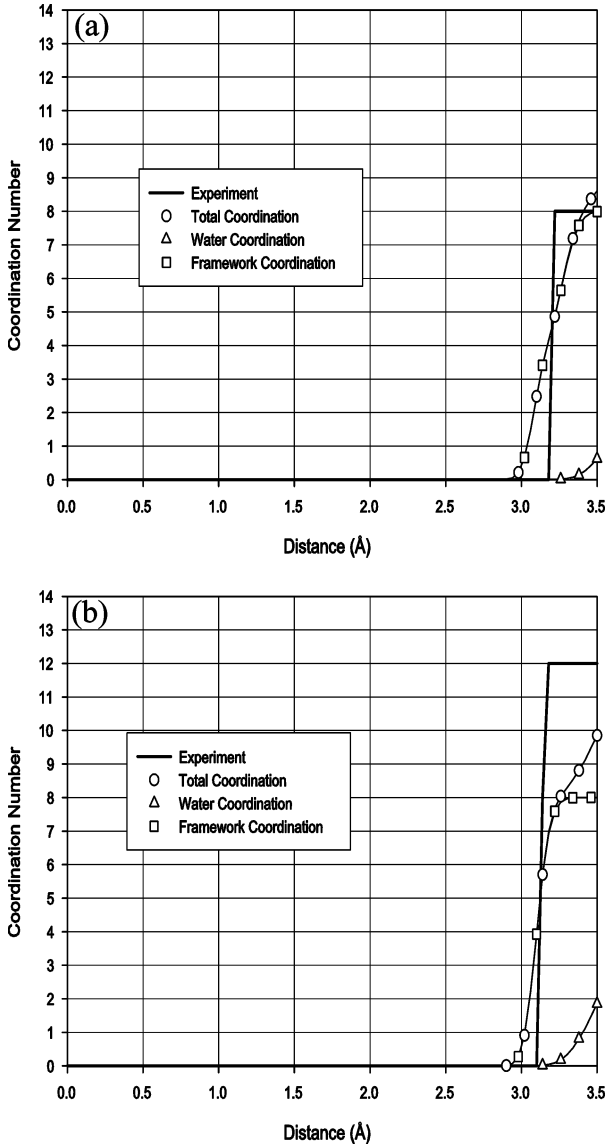


**Figure 6.** $Cs^+$ cation coordination number as a function of distance in (a) Cs−CST and (b) Cs−Nb−CST. $Cs^+$ gains additional coordination from neighboring water molecules in Cs−Nb−CST.

in Table 5. The shell and rigid ion models once again show very similar results. The Na2 and Na3 sites are very close to the two sodium/water positions found in the Na−CST stucture. Sodium in the Na2 site is observed to coordinate with 2 water molecules, 3 framework O1 oxygen atoms, and 0.8 framework O4 oxygen atoms at a distance of 2.90 Å, while sodium in Na3 coordinates with 1.2 water molecules, 3.7 framework O1 oxygen atoms, and 0.6 framework O2 oxygen atoms at a distance of 2.90 Å. In both sites, sodium is able to gain a high coordination with neighboring water molecules and framework oxygen atoms, thereby greatly increasing its stability.

Finally, we note that the simulations show a small, but nonnegligible amount of cesium located near the experimental O(W1) site. Likewise, there is a small amount of water located near the Cs1 site. We do not believe these positions are populated in the real material, but instead are a result of poor sampling in the simulations. The cesium is likely kinetically trapped in this position due to high amounts of sodium and water present within the tunnels. Even when simulating at the highest temperature with the simulated annealing method, it was difficult to observe cesium cations switch positions with water molecules, mainly because of the large ionic radius of cesium and the small diameter of the CST tunnels. Cesium is relatively unstable in the O(W1) site compared to the Cs1 site, because it can only coordinate with 1.3 oxygen atoms at 3.20 Å. Therefore, we expect that on experimental time scales, the cesium near O(W1) and water at Cs1 will be able to overcome the high energy barriers associated with swapping positions and move to their more energetically favorable Cs1 and O(W1) configurations, respectively. We expect that a Monte Carlo procedure, which can easily allow ions to "pass" each other in the one-dimensional tunnels would capture this effect.

The above results provide insight into the position of $Na^+$, $Cs^+$, and water in the base CST material. For Na−CST, the simulations provide an indication that water and sodium may share the Na2 and O(W2) sites, in contrast to the conclusion drawn from the X-ray experiments. For Cs−CST, the simulations agree well with experiments on the position of $Cs^+$ and water and give reasonable positions for the $Na^+$ that could not be detected with X-ray diffraction. Given the small differences between the results obtained using the rigid ion model and the shell model and the overall good agreement with experiment,

we conclude that the rigid ion model is able to accurately predict cation and water positions in this class of materials. Thus, only rigid ion model calculations were performed for the remaining two systems.

**4.3. Nb−CST.** There are two experimentally observed water sites in Nb−CST, O(W1) and O(W2). As before, framework Na1 sodium cations are present and constrained to their crystallographic positions. The simulated water postions agree very well with the experiments for this material, as shown in Table 6. Simulations predict that the first water site is fully occupied and located 0.19 Å from the experimental O(W1) site. Again, water near the O(W1) site coordinates with the framework Na1 sodium cations and hydrogen bonds with the O2 framework oxygen atoms. The remaining water is observed to locate near the experimental O(W2) site, although the difference between simulated and experimental position is 0.46 Å. The main difference is that simulated water associated with the O(W2) site are located closer to the center of the CST tunnels than what is observed experimentally, which is consistent with O(W2) locations in the Na−CST structure.

**4.4. Cs−Nb−CST.** Finally, for the Cs−Nb−CST structure, experiments indicate that there are two partially occupied cesium sites, Cs1 and Cs2, two water sites sites, O(W1) and O(W2), and one framework Na1 sodium site. Figure 2c shows the positions of Cs1, O(W1), and O(W2). The Cs2 site is located behind the Cs1 site and is not shown. The Cs1 cesium site is located at the (1/2, 1/2, 1/4) position and is highly coordinated with eight framework O1 atoms. Additionally, the experiments indicate that the cesium at the Cs1 site coordinates at 3.18 Å with between 0 and 4 water molecules from the partially occupied O(W2) site to give a total coordination number between 8 and 12.

The simulations show an almost perfect match with the experiments for the location of cesium in the Cs1 position, as seen in Table 6. However, there is no evidence of $Cs^+$ locating in the Cs2 site. Once again, we attribute this to the fact that the simulations do not account for lattice distortion effects and nonuniform compositions of cations and water molecules within the CST tunnels.

Cesium associated with the Cs1 site is found to coordinate with approximately eight framework O1 oxygen atoms at a distance of 3.26 Å (see Figure 6b). To gain the extra coordination that is observed experimentally, water must occupy the experimental O(W2) sites. The O(W2) site is located closer to the center of the tunnel as compared with the O(W1) site, but has the same *c*-axis coordinate. Although only one water molecule is observed to contribute additional coordination to cesium within 3.40 Å, simulations do show water locating between the O(W1) and O(W2) sites. Distribution plots of water in Cs−Nb−CST are given in Figure 7. Water is not as localized as it was in the Nb-free material and is able to easily move between the two water sites. This leads to a deviation between the computed and experimental positions of 0.38 Å for O(W1) and for O(W2). One reason for this discrepancy may be due to the use of an average T-atom model for niobium and titanium. Since an averaged T-atom model is used, the results may give an "averaged" water site rather than resolving water into two sites, as observed experimentally. The results are interesting, however, since they suggest that the addition of Nb to the framework forces water to leave the O(W1) site and increase the population of the O(W2) site. Water in the O(W2) site is able to provide additional stability to exchanged $Cs^+$, which may explain the experimental observation that the addition of Nb to CST increases cesium selectivity. Finally, there is a small

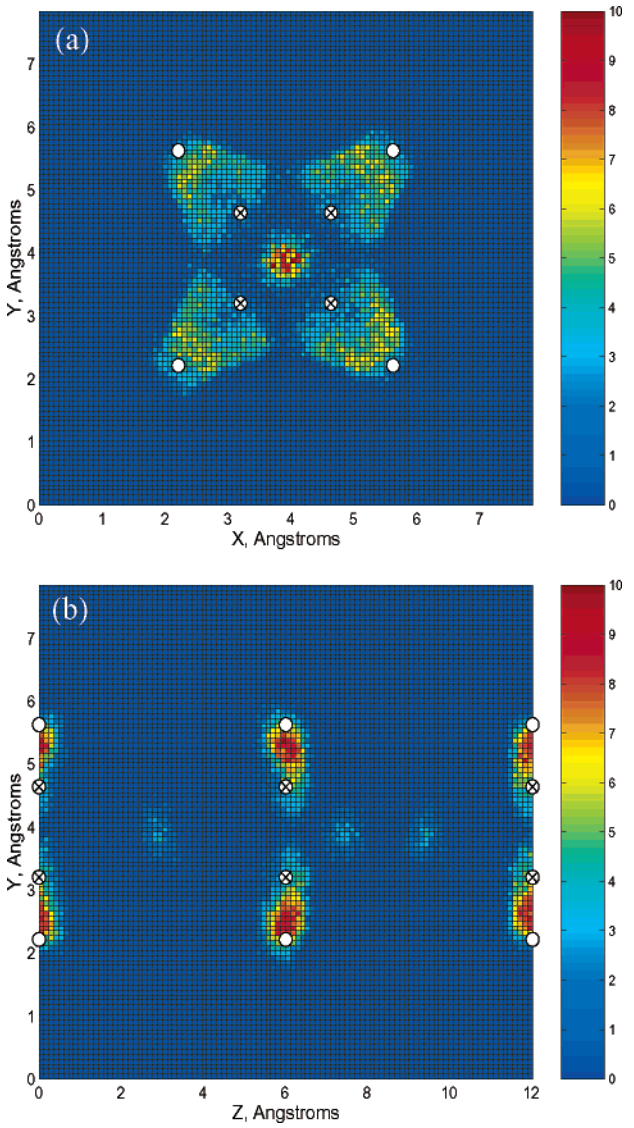


**Figure 7.** Distribution plot of the water molecules in one unit cell of Cs−Nb−CST along (a) the [001] direction and (b) the [100] direction at 300 K. The experimental O(W1) and O(W2) sites are represented by the open and crossed circles, respectively.

amount of water that was observed to locate near the experimental Cs1 sites. This was also observed experimentally,[8] where it is noted that an electron density is observed in the difference Fourier and can be attributed to water or minor amounts of sodium.

## 5. Conclusions

A new, transferable potential model has been developed which accurately predicts the preferred cation and water positions in CST ion exchange materials. The model has been tested using a simulated annealing molecular dynamics protocol. A comparison between the shell model and rigid ion model is given, where it is determined that although the rigid ion model neglects polarization effects, it is well suited for ion exchange simulations. In addition, the rigid ion model is able to simulate supercells, which avoids possible correlation effects that may arise due to periodic boundary conditions. The rigid ion model has been used to determine cation and water siting in all of the CST materials studied. In contrast to experimental X-ray diffraction studies, the simulations suggest that $Na^+$ and water both can reside in the Na2 and O(W2) positions. That is, in

addition to populating the Na2 position, $Na^+$ can populate the O(W2) position that was assigned experimentally as an exclusive water site. Moreover, while water exclusively populates the O(W1) position, it can also reside in the Na2 and O(W2) position. When $Cs^+$ exchange takes place in this material, the simulations find $Cs^+$ in the experimental Cs1 position. Simulations also predict the location of $Na^+$ in two positions not previously identified experimentally. When 25% of the Ti is substituted for Nb, the simulations show that $Cs^+$ is stabilized by water leaving the O(W1) site and entering the O(W2) site, where it can coordinate with $Cs^+$, thereby stabilizing the cation and leading to greater stability. This result supports the experimental observation that addition of Nb to the CST lattice increases cesium selectivity. In future work we shall apply similar methodology to a range of tunnel type ion exchangers to test the generality of the method.

**Acknowledgment.** This research was supported by the Environmental Management Science Program of the Office of Environmental Management, U.S. Department of Energy, Grant No. DE-FG07-01ER63282 (ND) and Grant No. DE-FG07-01ER63300 (TAMU).

## References and Notes

(1) Clearfield, A. *Chem. Rev.* **1988**, *88*, 125.
(2) Poojary, D. M.; Cahill, R. A.; Clearfield, A. *Chem. Mater.* **1994**, *6*, 2364.
(3) Anthony, R. G.; Dosch, R. G.; Gu, D.; Phillip, C. V. *Ind. Eng. Chem. Res.* **1994**, *33*, 2702.
(4) Zheng, Z.; Gu, D.; Anthony, R. G.; Klavetter, E. *Ind. Eng. Chem. Res.* **1995**, *34*, 2142.
(5) Poojary, D. M.; Bortun, A. I.; Bortun, L. N.; Clearfield A. *Inorg. Chem.* **1996**, *35*, 6131.
(6) Zheng, R. G.; Anthony, J. E.; Miller, J. E. *Ind. Eng. Chem. Res.* **1997**, *36*, 2427.
(7) Luca, V.; Hanna, J. V.; Smith, M. E.; James, M.; Mitchell, D. R. G.; Bartlett, J. R. *Microporous Mater.* **2002**, *55*, 1.
(8) Tripathi, A.; Medvedev, D.; Nyman, M.; Clearfield, A. *J. Solid State Chem.* **2003**, *175*, 72.
(9) Hill, J. R.; Freeman, C. M.; Subramanian, L. *Rev. Comput. Chem.* **2000**, *16*, 141.
(10) Fuchs, A. H.; Cheetham, A. K. *J. Phys. Chem. B* **2001**, *105*, 7375.
(11) Auerbach, S. M. *Int. Rev. Phys. Chem.* **2000**, *19*, 155.
(12) Fois, E.; Gamba, A.; Spano, E. *J. Phys. Chem. B* **2004**, *108*, 154.
(13) Ricchiardi, G.; de Man, A.; Sauer, J. *Phys. Chem. Chem. Phys.* **2000**, *2*, 2195.
(14) Titiloye, J. O.; Parker, S. C.; Stone, F. A.; Catlow, C. R. A. *J. Phys. Chem.* **1991**, *95*, 4038.
(15) Demontis, P.; Suffritti, G. B. *Chem. Rev.* **1997**, *97*, 2845.
(16) van Well, W. J. M.; Cottin, X.; Smit, B.; van Hooff, J. H. C.; van Santen, R. A. *J. Phys. Chem. B* **1998**, *102*, 3952.
(17) Bell, A. T.; Maginn, E. J.; Theodorou, D. N. *Handbook of Heterogeneous Catalysis*; Ertl, G., Knözinger, H., Weitkamp, J., Eds.; VCH: Weinheim, Germany, 1997; Vol 3, pp 1165−1188.
(18) Wang, Q.; Johnson, J. K. *J. Phys. Chem. B* **1994**, *103*, 277.
(19) Maddox, M. W.; Gubbins, K. E. *Int. J. Thermophys.* **1994**, *15*, 1115.
(20) Oumi, Y.; Matsuba, K.; Kubo, M.; Inui, T.; Miyamoto, A. *Microporous Mater.* **1995**, *4*, 53.
(21) Jentys, A.; Catlow, C. R. A. *Catal. Lett.* **1993**, *22*, 251.
(22) Grillo, M. E.; Carrazza, J. *J. Phys. Chem.* **1996**, *100*, 12261.
(23) Anderson, M. W.; Agger, J. R.; Luigi, D.; Baggaley, A. K.; Rocha, J. *Phys. Chem. Chem. Phys.* **1999**, *1*, 2287.
(24) Dick, B. G.; Overhauser, A. W. *Phys. Rev.* **1958**, *112*, 90.
(25) Jackson, R. A.; Catlow, C. R. A. *Mol. Sim.*, **1988**, *1*, 207.
(26) Higgins, F. M.; Watson, G. W.; Parker, S. C. *J. Phys. Chem. B* **1997**, *101*, 9964.
(27) de Leeuw, N. H.; Parker, S. C. *Phys. Rev. B* **1998**, *58*, 13901.
(28) Higgins, F. M.; de Leeuw, N. H.; Parker, S. C. *J. Mater. Chem.* **2002**, *12*, 124.
(29) Lewis, D. W.; Ruiz-Salvador, A. R.; Almora-Barrios, N.; Gomez, A.; Mistry, M. *Mol. Sim.* **2002**, *28*, 649.
(30) Hill, J.-R.; Minihan, A. R.; Wimmer, E.; Adams, C. J. *Phys. Chem. Chem. Phys.* **2000**, *2*, 4255.
(31) Jaramillo, E.; Auerbach, S. M. *J. Phys. Chem. B* **1999**, *103*, 9589.
(32) Buttefey, S.; Boutin, A.; Mellot-Draznieks, C. F.; Fuchs, A. H. *J. Phys. Chem. B* **2001**, *105*, 9569.
(33) Buttefey, S.; Boutin, A.; Fuchs, A. H. *Mol. Sim.* **2002**, *28*, 1049.
(34) Mellot-Draznieks, C.; Buttefey, S.; Boutin, A.; Fuchs, A. H. *Chem. Commun.* **2001**, *21*, 2200.
(35) Beauvais, C.; Guerrault, X.; Coudert, F. X.; Boutin, A.; Fuchs, A. H. *J. Phys. Chem. B* **2004**, *108*, 399.
(36) Vitale, G.; Mellot, L. M.; Bull, A. K.; Cheetham, A. K. *J. Phys. Chem. B* **1997**, *101*, 4559.
(37) Lignieres, J.; Newsam, J. M. *Microporous Mesoporous Mater.* **1999**, *28*, 305.
(38) Furukawa, S.; Goda, K.; Zhang, Y.; Nitta, T. *J. Chem. Eng. Jpn.* **2004**, *37*, 67.
(39) Faux, D. A. *J. Phys. Chem. B* **1999**, *103*, 7803.
(40) Prewitt, C. T.; Shannon, R. D. *Trans. Am. Crystallogr. Assoc.* **1969**, *5*, 57.
(41) Kiselev, A. V.; Lopatkin, A. A.; Schulga, A. A. *Zeolites* **1985**, *5*, 261.
(42) Woodley, S. M.; Battle, P. D.; Gale, J. D.; Catlow, C. R. A. *Phys. Chem. Chem. Phys.* **1999**, *1*, 2535.
(43) Kofke, D. A. *J. Chem. Phys.* **2002**, *117*, 6911.
(44) Gale, J. D. *J. Chem. Soc., Faraday Trans.* **1997**, *93*, 629.
(45) Allen, M. F.; Tildesley, D. J. *Computer Simulation of Liquids*; Oxford Science Publications: Oxford, 1987.